Urban-rural interactions in a South Korean forest in ozone and oxygenated volatile organic compound formation perspectives

[1]Saewung Kim, [2]So-Young Kim, [3]Meehye Lee, [3]Heeyoun Shim, [4,5]Glenn M. Wolfe, [6]Alex B. Guenther, and [1]Amy He, [2]Youdeog Hong, [2]Jinseok Han

1 Department of Earth System Science, School of Physical Sciences, University of California, Irvine, Irvine California, 92697 U.S.A.
2 National Institute Environmental Research, Incheon, South Korea
3 Department of Earth and Environmental Sciences, Korean University, Seoul, South Korea
4 Joint Center for Earth Systems Technology, University of Maryland Baltimore County, Baltimore, MD, USA
5 Atmospheric Chemistry and Dynamics Laboratory, NASA Goddard Space Flight Center, Greenbelt, MD, USA
6 Atmospheric Sciences and Global Change Division, Pacific Northwest National Laboratory, Richland WA USA

To be submitted to Atmospheric Chemistry and Physics “East Asian Megacity” Special Issue

Abstract

Rapid urbanization and economic development in East Asia in past decades has led to photochemical air pollution problems such as excess photochemical ozone and aerosol formation. Asian megacities such as Seoul, Tokyo, Shanghai, Gangzhou, and Beijing are surrounded by densely forested areas and recent research has consistently demonstrated the importance of biogenic volatile organic compounds (VOCs) from vegetation in determining oxidation capacity in the suburban Asian megacity regions. Uncertainties in constraining tropospheric oxidation capacity, dominated by hydroxyl radical concentrations, undermine our ability to assess regional photochemical air pollution problems. We present an observational dataset of CO, NO_X, SO_2, ozone, HONO, and VOCs (anthropogenic and biogenic) from Taehwa Research Forest (TRF) near the Seoul Metropolitan Area (SMA) in early June 2012. The data show that TRF is influenced both by aged pollution and fresh BVOC emissions. With the dataset, we diagnose HOx (OH, HO_2, and RO_2) distributions calculated using the University of Washington Chemical Box Model (UWCM v 2.1) with near-explicit VOC oxidation mechanisms from MCM 3.2 (The Master Chemical Mechanism). Uncertainty from unconstrained HONO sources and radical recycling processes highlighted in recent studies is examined using multiple model simulations with different model constraints. The results suggest that 1) different model simulation scenarios cause systematic differences in HO_X distributions especially OH levels (up to 2.5 times) and 2) radical destruction (HO_2+HO_2 or HO_2+RO_2) could be more efficient than radical recycling (HO_2+NO) especially in the afternoon. Implications of the uncertainties in radical chemistry are discussed with respect to ozone-VOC-NO_X sensitivity and VOC oxidation

product formation rates. Overall, the VOC limited regime in ozone photochemistry is assessed but the degree of sensitivity can significantly vary depending on the model scenarios. The model results also suggest that RO_2 levels are positively correlated with oxygenated VOCs (OVOCs) production that is not routinely constrained by observations. These unconstrained OVOCs can cause higher than expected OH loss rates (missing OH reactivity) and secondary organic aerosol formation. The series of modeling experiments constrained by observations strongly urge observational constraint of the radical pool to enable precise understanding of regional photochemical pollution problems in the East Asian megacity region.

1. Introduction

NOx ($NO+NO_2$) and volatile organic compounds (VOCs) are two important precursors that drive HOx radical cycles(Levy, 1971). In the presence of NO_X, VOC oxidation processes recycle OH and produce photochemical oxidation products such as ozone and oxygenated VOCs (OVOCs). This reaction cycle is highly non-linear. For example, excess NO_2 may expedite nitric acid formation (R1), limiting ozone production. In the same context, excess VOCs may expedite peroxy radical production (R2), which limits OH regeneration from peroxy radicals.

$$OH + NO_2 + M \rightarrow HNO_3 + M \quad (R1)$$

$$HO_2 + RO_2 \rightarrow ROOH \quad (R2)$$

The non-linearity in tropospheric photochemistry has been relatively well studied in the urban regions of developed countries and applied in ozone reduction policy. The Los Angeles Metropolitan Area has accomplished significant ozone reduction by implementing aggressive emission reductions of both NOx and VOC especially from mobile sources (Ryerson et al., 2013). The remarkable ozone abatement was possible due to the fact that there is no significant pollution transport from other metropolitan areas and no significant natural emission sources especially volatile organic compounds from vegetation (BVOCs; biogenic volatile organic compounds) compared with anthropogenic VOC mostly from mobile sources (Pollack et al., 2013;Huang et al., 2013). In the late 80s, Trainer et al. (1987) first demonstrated the importance of isoprene (C_5H_8) as a peroxy radical source that can contribute significant ozone production in rural areas. The

101 importance of isoprene in ozone production in urban areas has also been highlighted, e.g.
102 in the Atlanta Metropolitan Area (Chameides et al., 1988).
103 Isoprene is a hemiterpenoid species and is the globally dominant VOC emission
104 from vegetation (Arneth et al., 2011;Guenther, 2013). Arguably, isoprene is the most
105 frequently studied BVOC from the perspective of atmospheric oxidation processes and
106 their implications for ozone and aerosol formation. However, significant uncertainty
107 hinders assessing the roles of isoprene in regional and global photochemistry in three
108 fronts. First, there is still significant uncertainty in estimating emission rates from each
109 individual plant species on regional scales (Guenther, 2013). Second, limited isoprene
110 inter-comparison results (Barket et al., 2001) suggest that there are large systematic
111 biases among different analytical techniques. Lastly, recent laboratory, theoretical and
112 field observations suggest significant uncertainty in tropospheric isoprene oxidation
113 processes initiated by OH. Until early 2000, it was thought that three first generation
114 isoprene oxidation products (methyl vinyl ketone, methacrolein, and formaldehyde) from
115 OH oxidation were enough to constrain isoprene tropospheric oxidation processes for
116 modeling purposes (e.g. Spaulding et al., 2003). This is an interesting evolution of
117 thoughts considering that Paulson and Seinfeld (1992), one of pioneering works
118 describing isoprene oxidation, clearly claimed that 22 % of first generation isoprene
119 oxidation products from the reaction with OH was not identified and likely included
120 multifunctional C5 compounds. Recent advances in analytical techniques (Kim et al.,
121 2013a) have shown that indeed significant C5-hydroxy carbonyl (e.g. isoprene
122 hydroperxyenals, HPALD) and peroxide compounds are produced as first generation
123 isoprene oxidation products (Crounse et al., 2011;Paulot et al., 2009;Wolfe et al.,

2012;Zhao and Zhang, 2004) and are a strong function of NO concentrations (Peeters and Muller, 2010). In general, low to intermediate NO levels (~ 100 pptv or lower), the yields of C5-hydroxy carbonyl compounds become higher. These new findings in the isoprene oxidation process are also closely related with recent findings in unexpectedly high OH concentrations (Hofzumahaus et al., 2009;Lelieveld et al., 2008) and substantial missing OH sinks also known as unexpectedly high OH reactivity in high isoprene environments (Di Carlo et al., 2004;Edwards et al., 2013;Kim et al., 2011;Lou et al., 2010).

These new findings have significant implications in regional air quality especially in photochemical ozone and SOA production. Despite the strong anthropogenic pollutant emissions in East Asia (China, Japan and South Korea), recent research has shown that isoprene accounts for a major OH chemical sink in suburban areas near Beijing (Ran et al., 2011), the Pearl River Delta region (Lu et al., 2012), and Seoul (Kim et al., 2013d;Kim et al., 2013b). Consequently, modeling studies also clearly show that isoprene contributes significantly to ozone formation in Asian megacity regions. Kim et al. (2013d) reported that simulated ozone levels with isoprene chemistry are up to 30 % higher than ozone simulation without isoprene chemistry using the WRF-Chem model, indicating an urgent need to implement improved isoprene chemistry schemes in these models in order to simulate the unexpected higher levels of OH in isoprene rich environments. This is especially alarming as Hofzumahaus et al. (2009) reported significantly higher (~ 2.6 times at noon) than expected OH levels in the Pearl River Delta region in China. Therefore, the current assessments based on the conventional OH photochemistry could significantly misdiagnose regional air-quality status and mislead policy implementation to reduce photochemical air pollution in the East Asian region. Furthermore, as the

147 importance of BVOC in regional air-quality issues in ozone and SOA formation has been
148 also highlighted in Europe and North America, the uncertainty in isoprene
149 photochemistry has significant implications in urban and suburban air quality in
150 general(Zhang et al., 2008a;Sartelet et al., 2012).

151 We present atmospheric observations of NO_X, CO, VOCs, ozone, and HONO in
152 the Taehwa Research Forest (TRF) in the Seoul Metropolitan Area (SMA), South Korea.
153 We use these data to conduct observationally constrained box model (University of
154 Washington Chemical Box Model; UWCM) calculations to estimate OH, HO_2 and RO_2
155 concentrations with different sets of observational parameters. We discuss current
156 uncertainty in OH-isoprene photochemistry with perspectives of constraining
157 photochemical ozone production and OVOCs precursors of secondary organic aerosols.
158

159 2. **Methods**

160 The Taehwa Research Forest (TRF) is located ~ 35 km from the center of Seoul,
161 South Korea. The TRF is located at the southeastern edge of the Seoul metropolitan Area
162 (SMA, population of ~ 23 million). TRF has a sampling tower located in the middle of a
163 coniferous tree plantation (200 m by 200 m) with the canopy height of 18 m (*Pinus*
164 *koraiensis*) surrounded by a deciduous forest mostly composed by oak. Kim et al. (2013d)
165 reported CO, NO_X, SO_2, ozone, and VOC observation results along with WRF-Chem
166 assessments of ozone forming potential of isoprene photochemistry. The report found that
167 isoprene was the most dominant OH chemical sink during daytime among the observed
168 trace gases and explained up to 30 % of ozone production. The TRF instrumentation has

169 previously been described by Kim et al. (2013d). Therefore, just brief descriptions of
170 analytical techniques are given in this paper.
171
172 **2.1. CO, NO_X, SO_2, ozone, VOCs, and meteorological parameters**
173 Thermo Fisher Scientific Enhanced Trace Level Gas Analyzers are used for CO,
174 NO_X, SO_2, and ozone observations as summarized Table 1. VOC observations are
175 conducted by a High-Sensitivity Proton Transfer Reaction-Mass Spectrometer (PTR-MS,
176 Ionicon GmbH). The atmospheric application of this technique is thoroughly reviewed by
177 de Gouw and Warneke (2007). In addition, the instrument suite at TRF is thoroughly
178 described in (Kim et al., 2013d). PTR-MS can quantify atmospheric VOCs that have
179 higher proton affinity than the proton affinity of H_2O (691 kJ mol^{-1}). Most alkanes have
180 lower proton affinity than water but alkene, aromatic and some OVOCs have higher
181 proton affinity and are suitable for quantification using PTR-MS (Blake et al., 2009).
182 These compounds are more reactive than alkane compounds so PTR-MS has capability to
183 observe reactive atmospheric compounds. The TRF PTR-MS system was set to measure
184 acetaldehyde, acetone, acetic acid, isoprene, methylvinylketone (MVK) + methacrolein
185 (MACR), MEK, benzene, xylene (*p*, *m*, and *o*), and monoterpenes (MT). Each compound
186 was set to be monitored for 1 second each resulting in a sample cycle of 15 seconds.
187 Lower detection limits for the observed VOCs are estimated to be 20 ppt for a 5 second
188 integration with sensitivity of 70 counts ppb^{-1}. (2 σ). Meteorological parameters such as
189 temperature and humidity are monitored by LSI LASTEM Meteorological Sensors. All
190 the presented data is from the 15 m (the canopy height is 18 m) sampling line and
191 meteorological sensors collocated at this height too.

PTR-MS with a quadrupole mass filter has an intrinsic limitation that isobaric compounds are all collectively quantified with the same channel (m/z) with a resolution of unit mass. This limitation particularly becomes an issue for investigating the roles of different isomers of MT and sesquiterpenes (SQTs) in photochemistry. For this reason, we also occasionally collect sorbent cartridge samples to analyze MT and SQT speciation in both ambient air and branch enclosure emissions near the sampling tower. As described in (Kim et al., 2013d), Tenax GR and Carbotrap 5TD packed sorbent cartridges (Markes Int, Llanstrisant, UK) were used for sampling. The sampled cartridges were shipped to National Center for Atmospheric Research (NCAR), Boulder CO, USA for gas chromatography-mass spectrometer (GC-MS) analysis. An Agilent 7890 GC/5975 C Electron Impact Mass Spectrometer (GC-MS/FID) in conjunction with a MARKES Unity1/Ultra thermal desorption system optimized for terpenoid analysis quantifies speciated MT and SQT in the sorbent samples. Cartridge samples are both collected from ambient and branch enclosure air. Ambient samples were collected in the mid-day to early afternoon with a volume of 6 L. Ozone in the ambient air was removed using a Na_2SO_3 filter. Branch enclosure samples were also collected in the mid-day time frame with a volume of 1 L without an ozone filter as zero air was introduced to the branch enclosure. We present these analytical results from GC-MS analysis limited to the qualification purpose to examine MT and SQT speciation.

2.2 HONO quantification

HONO was measured with an ion chromatography (IC) coupled with diffusion scrubber. Air was introduced to diffusion scrubber (Lab solutions Inc., IL, USA) through

215 a 2 m PFA tubing (1/4" i.d.) at 1.5 L m^{-1} using a filtered orifice restrictor (F-950, air
216 logic, WI, USA). Air flowing through diffusion scrubber interfaced with deionized water,
217 into which HONO was extracted. 50 μL of solution was injected into the IC system
218 through a PEEK loop (Rheodyne, WA, USA) and 6-way valve (EV750-100, Rheodyne,
219 WA, USA). Eluent was a mixture of Na_2CO_3 and $NaHCO_3$, which was pumped by a
220 HPLC pump (DX-100, Dionex, CA, USA) into a guard column (Ionpax® AG 14,
221 4x50mm, Dionex, CA, USA) and then analytical column (Ionpax® AS 14, 4x250mm,
222 Dionex, CA, USA). The column affluent passed through a suppressor (ASRS 300,
223 Dionex, CA, USA) and HONO was detected as nitrite ion in conductivity detector (550,
224 Alltech, IL, USA). The entire measurement processes of sampling, chemical analysis, and
225 data acquisition were controlled by a digital timer and data acquisition software
226 (DSchrom-n, DS science, Korea), by which we obtained two measurements every hour.
227 The system was calibrated using a NO_2^- standard solution (Kanto chemical Co., Inc.,
228 Tokyo, Japan) whenever reagents were replaced. The detection limit was 0.15 ppb
229 estimated from 3σ of the lowest working standard. Specific analytical characteristics are
230 described in Simon and Dasgupta (1995) and Takeuchi et al. (2004).
231
232 **2.3 UWCM box model**
233 UWCM 2.1 is an open source box model coded by MATLAB (MathWorks®).
234 The model platform can be downloaded from a website
235 (http://sites.google.com/site/wolfegm/code-archive). The box model is embedded its own
236 HO_X ($OH+RO_2$)-RO_X (peroxyradical and alkoxy radical)-NO_X coupling chemical
237 mechanism. UWCM utilizes Master Chemical Mechanism version 3.2 (MCM 3.2)

238 (Jenkins et al., 1997; Saunders et al., 2003) for near-explicit VOC photo-oxidation
239 schemes. A more detailed model description can be found in Wolfe and Thornton (2011).
240 To minimize uncertainty from the parameterizations of transport and emission, we
241 constrained relatively long-lived trace gases presented in Figure 1. This box modeling
242 technique has been commonly used for examination of OH levels that can be justified by
243 the short chemical lifetime of OH (Kim et al., 2014;Kim et al., 2013c;Mao et al.,
244 2012;Mao et al., 2010). Recently developed isoprene photo-oxidation mechanisms
245 shown in Archibald et al. (2010) are also incorporated in the model. In addition, Kim et al.
246 (2013c) and Wolfe et al. (2013) applied the model in the identical fashion as used for this
247 study to probe radical distributions using comprehensive observational datasets. This
248 study used the UWCM to simulate the diurnal variations of radical pool ($OH+HO_2+RO_2$)
249 distributions as observational parameters such as CO, NO_X, ozone, and VOCs are
250 constrained. To fully account for roles of OVOCs in the box model as radical sources, we
251 simulated three consecutive days and presented diurnal variations from the third day. The
252 specific parameters, constrained by observations are listed above.
253
254 **3. Results**
255 **3.1. Observational Results**
256 Diurnal averages of observed trace gases (June 1st 2012 to June 6th 2012) are
257 shown in Figure 1. The TRF observatory is in continuous operation and we choose this
258 six day period because a regional high-pressure system caused a stagnant air pollution
259 event in this period. In the center of Seoul (the real-time data available at
260 http://www.airkorea.or.kr), carbon monoxide was observed in the similar levels during

261 the focused period (June 1st to June 6th, 2012). On the other hand, the NO_2 level observed
262 in central Seoul was much higher (20-50 ppb) compared with observed levels at TRF.
263 The reason can be attributed to differences between the chemical lifetime of CO (~a
264 month) and NO_2 (~a few hours to a day). The observations also clearly indicate that the
265 TRF is not directly influenced by fresh SMA pollution plumes although the TRF is very
266 close to the center of Seoul (30 km away from the city center) and a regional modeling
267 study shows most of CO and NO_X sources are located in the city center (Ryu et al., 2013).
268 Similar observations were also reported for other East Asian megacities such as Beijing
269 (Ma et al., 2012), where ~ 30 ppb and ~ 15 ppb of NO_2 were observed at noon in the
270 urban and the adjacent rural sites, respectively. In contrast, there were no noticeable
271 differences in CO levels between the urban and rural sites (~ 1-2 ppm). The observed
272 CO, NO_X and SO_2 levels in TRF were much lower than those observed in the suburban
273 regions of Chinese megacities such as Beijing (Ma et al., 2012), Shanghai (Tie et al.,
274 2013), and the Pearl River Delta Region (Lu et al., 2012) and similar with the observed
275 levels in Tokyo, Japan (Yoshino et al., 2012).
276 Previous VOC observations in the SMA consistently have shown that toluene is
277 the dominant anthropogenic VOC followed by other aromatic compounds such as xylene
278 and benzene (Kim et al., 2012;Na and Kim, 2001). Na and Kim (2001) reported high
279 concentrations of propane from house hold fuel use. However, recent observation results
280 from the photochemical pollution observational network managed by National Institute of
281 Environmental Research (NIER) of South Korea in the SMA clearly indicate that propane
282 levels have declined and are now much lower than the levels previously observed (NIER,
283 2010). This is probably caused by the implementation of a policy changing household

284 fuel sources from propane to methane. (Kim et al., 2012) presented detailed aromatic
285 VOC distributions in the SMA from four different urban observational sites. In average,
286 toluene concentrations were observed ~ 7 times higher than the observed levels of xylene
287 and benzene. At the TRF, a similar anthropogenic VOC speciation distribution was
288 observed as shown in Figure 1. The observed toluene and MEK (methyl ethyl ketone)
289 mixing-ratios were much higher than benzene and xylene. MEK is detected in m/z of 73^+
290 by PTR-MS. Although methyl glyoxal, an atmospheric VOC oxidation product, is also
291 detected on the same mass, we assumed that 73^+ of m/z signals are mostly from MEK, an
292 anthropogenic VOC, since the temporal variation follows that of anthropogenic VOC
293 such as toluene and xylene. In addition, atmospheric lifetime of methyl glyoxal is much
294 shorter than MEK.
295 As the observation facility is located in the middle of a pine tree plantation (*Pinus*
296 *koraiensis*), monoterpenes (MT) are consistently observed. The temporal variation of
297 monoterpenes is affected by the planetary boundary layer evolution with a pattern of
298 higher MT levels during night than those of mid-day as has been often reported in other
299 forest environments (Bryan et al., 2012;Kim et al., 2010) This can be explained by
300 interplays between boundary layer evolution and temperature dependent MT emission. It
301 should be noted that the branch enclosure BVOC emission observations indicate that the
302 daily maxima of MT and SQT emissions were observed in the midday (between noon to
303 2 pm in the local time. The observed MT and SQT speciation information is summarized
304 in Table 2. Table 2a summarizes branch enclosure sample analysis results and ambient
305 sample analysis results are summarized in Table 2b. In general, observed MT and SQT in
306 the ambient air are consistent with previously observed distributions (Kim et al., 2013d).

307 α-pinene and β-pinene were the dominant monoterpene and longifolene was the only
308 detected SQT species. In contrast, the branch enclosure observation results, reflecting
309 BVOC emission, indicate high emission of very reactive MT and SQT species such as β-
310 myrcene, α-caryophyllene, and β-caryophyllene. The fast oxidation of these highly
311 reactive terpenoid species suppresses the atmospheric presence of the compounds.
312 Therefore, photochemical oxidation processes of these compounds may have been
313 neglected. Investigating emissions and photochemistry of these reactive terpenoid
314 compounds can constrain potential missing OH reactivity and SOA production from
315 highly oxidized reaction products.

316 Isoprene is produced from carbon recently fixed through photosynthesis resulting
317 in higher emissions and atmospheric concentrations during the daytime. The temporal
318 variation shown in Figure 1 reveals an isoprene concentration maximum between 17:00
319 to 20:00. In addition, the ratios of MVK+MACR, major isoprene oxidation products and
320 isoprene at this period, are significantly lower than those of late morning to early
321 afternoon. Further regional and 1-D modeling studies are being conducted to examine
322 this observed temporal variations of isoprene and MVK+MACR. However, enhanced
323 isoprene levels in the late afternoon or early evening have been also reported in previous
324 studies (Apel et al., 2002;Bryan et al., 2012). The branch enclosure observations
325 demonstrate that isoprene is not emitted from the pine plantation but rather transported
326 from surrounding broadleaf forests as right outside of the pine plantation (200 m × 200 m)
327 is a forested area dominated by oak trees. Oak comprises 85 % of broadleaf trees in South
328 Korea (Lim et al., 2011). Lim et al. (2011) quantified isoprene emission rates for five
329 representative oak species in South Korea and report a wide emission range from oaks

330 that are negligible isoprene emitters (<0.004 μgC dw^{-1} h^{-1}; standard emission rates) to
331 others with very high isoprene emission rates of 130 μgC dw^{-1} h^{-1}.
332 Contributions from each observed trace gas species towards ambient OH
333 reactivity are shown in Figure 2. This is calculated as the product of the observed species
334 concentration and its rate constant for reaction with OH. Observed OH reactivity from
335 VOCs are much higher than from other trace gases such as CO, NOx, SO_2, and ozone.
336 Among the observed VOC species, BVOCs such as isoprene, α-pinene and β-pinene
337 accounted for significantly higher OH reactivity in comparison with the observed
338 AVOCs such as toluene, benzene, xylene and MEK. Isoprene accounts the highest OH
339 reactivity especially during the daytime. This analysis is consistent with reports from
340 other suburban observations from East Asian megacities such as Beijing (Ran et al.,
341 2011) , the PRD region, China (Lou et al., 2010), and the Kinki region Japan (Bao et al.,
342 2010).
343 HONO levels up to 1 ppb were observed in the early morning and were
344 consistently higher than 0.5 ppb during the daytime. These observed levels are
345 substantially higher than reported observations from forest environments in North
346 America (Ren et al., 2011;Zhou et al., 2011), where NO_X (~ 1 ppb) is substantially lower
347 than the level observed at TRF. Ren et al. (2011) reported 30 – 60 ppt of HONO at the
348 Blodgett Forest Research Station in the western foothills of the Sierra Nevada Mountains
349 in the late summer of 2007. Zhou et al. (2011) also reported the similar levels of HONO
350 (below 100 ppt) from the PROPHET forest, a mixed hardwood forest in northern
351 Michigan (Pellston, MI). However, significantly higher HONO levels (~ 200 ppt to ~ 2
352 ppb) were reported by Li et al. (2012) from a rural observational site in the Pearl River

353 Delta region near Guangzhou, where comparable NO_2 levels with TRF were observed.
354 The high HONO levels (a few hundred ppt) especially during the daytime have been
355 consistently reported near Eastern Asian megacities such as Beijing (Li et al., 2012),
356 Shanghai (Hao et al., 2006), and Seoul (Song et al., 2009). Still these are limited datasets
357 and further comprehensive analysis, especially more extensive observation is required.
358 However, two recently proposed HONO production mechanisms may be able to explain
359 the higher levels in the Eastern Asian megacity region. One is HONO production from
360 NO_2 photo-excitation (Wong et al., 2012) as the region usually has high NO_2
361 concentrations and the other is HONO emission from soil bacteria (Oswald et al., 2013).
362 Oswald et al. (2013) found differences as much as two orders of magnitude in HONO
363 emissions from soil samples from different environments (e.g. pH and nutrient contents).
364 In addition, as most of observations in the East Asia regions were conducted with ion
365 chromatography based methods, more direct HONO quantification techniques such as a
366 chemical ionization mass spectrometry technique (Roberts et al., 2010) need to be used to
367 characterize any potential interferences such a high NO_X environment (e.g. N_2O_5).
368
369 **3.2 HO_X Model calculations with different isoprene photo-oxidation scenarios and**
370 **the roles of unconstrained HONO sources in HO_X model evaluations.**
371 The presented observational results are used to constrain the UWCM box model.
372 We evaluate uncertainties in the tropospheric oxidation capacity and how it affects our
373 ability to constrain ozone and OVOCs, secondary aerosol precursor production. The
374 observational results clearly indicate that isoprene is the most dominant OH sink among
375 the observed VOCs. In addition, NO concentrations were higher in the 600 to 800 ppt

range in the morning. On the other hand, afternoon levels were substantially lower in the 50 to 100 ppt range. The environment provides a unique opportunity to examine implications of isoprene photochemistry in various NO conditions.

We conducted model simulation under six different scenarios. Each scenario is described in Table 3. The quantitative assessments of the impacts to radical concentrations (OH, HO_2, and RO_2) from unconstrained HONO sources are evaluated by examining the model outcomes of the scenarios with and without constraining observed HONO. To evaluate the impacts of hydroperoxy-methyl-butenal (HPALD) photolysis and isoprene peroxy radical recycling in the radical pool, each chemical mechanism is selectively constrained by different scenarios. For HPALD chemistry, we adapted two different HPALD formation rate constants published by Peeters and Muller (2010) and Crounse et al. (2011). The formation rates from Peeters and Muller (2010) is about 40 times faster than those from Crounse et al. (2011) in 298 K. Finally, we applied 2.6 of the OH yield from isoprene peroxy radical and HO_2 reactions for the evaluation (Wolfe et al., 2011). Although, Liu et al. (2013) demonstrated significantly lower OH recycling contributions from HO_2 + isoprene peroxy radical reactions than those argued by Wolfe et al. (2011) by interpreting chamber experiment results, the high recycling rate by Wolfe et al. (2011) is applied in the model calculations to explore upper limit of uncertainty in radical estimations.

Modeled OH, HO_2, and RO_2 from the five different model scenarios are shown in Figure 3. A summary of averaged OH, HO_2, and RO_2 concentrations in the morning (08:00 – 11:00) and the afternoon (13:00 – 16:00) from each simulation is shown in Table 4. With respect to the base run results (Scenario I), Scenario III with the lower

HPALD formation rate does not cause noticeable differences in radical concentrations. Adapting higher HPALD formation rates (Scenario II) cause significant differences in radical distribution especially in RO_2. This difference is likely caused by the fact that significant isoprene peroxy radical is converted to HPALD. The higher levels of discrepancy is found in RO_2 between Scenario I and Scenario II in the afternoon when low NO concentrations are observed, which efficiently facilitates HPALD formation. Adding HO_2+isoprene peroxy radical reactions as OH recycling processes (Scenario IV and V) results in significant enhancements in OH and HO_2 with respect to the base run (Scenario I). RO_2 concentrations are calculated in significantly different levels between Scenario IV and V. This can be again accounted by the applications of different HPALD formation rates in the two different model scenarios. The higher level of OH from the additional recycling process causes substantially higher RO_2 formation rates than those from the scenarios without the additional recycling process. The faster HPALD formation in Scenario IV is appeared to cause faster loss of RO_2 resulting in low RO_2 concentrations.

Most striking differences can be found model simulation results with or without constraining observed HONO as shown in Figure 3. Model calculation results from Scenario VI indicate significantly smaller OH, HO_2, and RO_2 concentrations than the concentrations calculated from the counter part (Scenario IV), which contains identical constraints and isoprene photochemistry except constraining observed HONO . Again, this clearly indicates that more thorough evaluations not only impacts of HONO to air quality but also analytical techniques should be followed to precisely constrain photochemical processes in the region as argued in section 3.1.

422

423 3.3 Implications of uncertainty in HO_X model calculations in assessing photochemical
424 ozone and OVOC production.

425 Two competing chemical reactions (R3 vs. R4,5,6) determine radical distribution
426 regimes.

427 $$RO_2 + NO \rightarrow RO + NO_2 \quad (R3)$$

428 $$RO_2 + HO_2 \rightarrow ROOH + O_2 \quad (R4)$$

429 $$RO_2 + RO_2 \rightarrow ROOR + O_2 \quad (R5)$$

430 $$HO_2 + HO_2 \rightarrow H_2O_2 + O_2 \quad (R6)$$

431

432 When the rate of R3 gets much faster than the sum of reaction rates of R4, R5,
433 and R6 then radical recycling processes become more efficient than radical destruction
434 processes. In this radical recycling regime, OH, a universal tropospheric oxidant, is well
435 buffered to maintain the elevated OH levels. On the other hand, the radical destruction
436 regime can be defined when the radical recycling rates (R3) are slower than the radical
437 destruction reaction rates (R4+R5+R6). Although it is still controversial the yield of OH
438 from (R4) for isoprene peroxy radicals which demands a serious discussion whether we
439 should regard R4 as a radical destruction reaction, we stick with the classical
440 categorization for radical recycling and destruction regimes in this study. The temporal
441 variations of radical-radical reaction rates from the model simulation scenarios are shown
442 in Figure 4. In general, the radical reaction rates are elevated as much as twice once
443 observed HONO is constrained in the model calculations (e.g. Scenario VI). This is
444 because unaccounted HONO in the model calculations cause significant underestimations

445 in the radical pool ($OH+HO_2+RO_2$) size with respect to the constrained HONO scenarios
446 as shown in Figure 4. In addition, as we include recently developed isoprene radical
447 chemistry, the RO_2+HO_2 reaction rates, known for a radical destruction pathway becomes
448 more faster. This is more conspicuous in the afternoon when NO concentration becomes
449 lower. The $RO_2 + HO_2$ reaction rates get higher than those of $RO_2 + NO$ in the afternoon
450 for the Scenario IV and V. This is surprising, as the radical destruction regime is usually
451 associated with low NO_X conditions. Suburban regions of megacities including the TRF
452 in general show high NO_X conditions. However, radical recycling rates are determined by
453 concentrations of NO. The fraction of NO in the NO_X pool is determined by competing
454 reactions between NO_2 photolysis and oxidation reactions of NO by ozone, HO_2, and
455 RO_2 radicals. Once we assume the pseudo-steady state of NO, then NO in NO_X pool can
456 be expressed as
457
458 $$[NO] = J_{NO2}[NO_2]/(k_{NO+O3}[O_3] + k_{NO+HO2}[HO_2] + k_{NO+RO2}[RO_2]) \quad (R6)$$
459
460 This mathematical expression clearly shows that NO levels are dependent on NO_X
461 mostly composed of NO_2. At the same time, the fraction of NO in NO_X is anti-correlated
462 with ozone, HO_2, and RO_2 concentrations. Therefore, the size of the radical pool
463 composed of HO_2 and RO_2 is relevant for determining the fractions of NO in given NO_X
464 levels. High HO_2 and RO_2 are likely observed in high VOC regions such as forested areas.
465 This could cause a smaller fraction of NO in the given NO_X pool so radical recycling gets
466 relatively weaker compared with radical destruction reaction pathways. More quantitative

467 approaches are required to categorize radical reaction pathways rather than qualitative
468 categorization such as high or low NO_X regimes.
469 High and low NO_X regimes also have been widely used to define ozone
470 production regimes. As NO_X catalyzes ozone production and peroxy radicals expedite
471 NO_X turnover, in general, higher NO_X and VOCs conditions result in higher ozone
472 production. However, non-linearity in photochemistry of ozone production causes a
473 complexity in ozone reduction strategy (Seinfeld, 1989). Conventionally, efficient ozone
474 production can be achieved by the balance between nitric acid production rates (P_{HNO3},
475 $OH + NO_2$) and peroxide production rates (P_{ROOH}, HO_2+RO_2 or P_{H2O2} HO_2+HO_2)
476 (Sillman and He, 2002). The imbalance will cause ozone production sensitivity towards
477 either NOx or VOCs. A comprehensive photochemical model analysis (Tonnesen and
478 Dennis, 2000b, a) demonstrated that in a wider range of ozone concentrations, the VOC
479 and NOx limited regimes can be determined by the ratios of P_{H2O2} and P_{HNO3}. The ratio
480 range (P_{H2O2}/P_{HNO3}) of 0.35 is regarded as the border range. In the VOC limited regime
481 ($P_{H2O2}/P_{HNO3} < 0.35$), ozone production is expected to decrease with increasing NO_X and
482 increase with increasing VOCs. In the NO_X limited regime ($P_{H2O2}/P_{HNO3} > 0.35$), ozone
483 production gets efficient with increasing NO_X and is insensitive to changes in VOCs
484 (Sillman and He, 2002). This categorization has guided policy-making processes whether
485 NO_X or VOC controls will be more effective in ozone reduction. A series of modeling
486 studies have been conducted to characterize ozone production regimes in the suburban
487 regions of East Asian megacities and have consistently concluded that the role of
488 isoprene is important in ozone production. However, most of these studies have
489 concluded that East Asian megacity regions are mostly in the VOC limited regime (Tseng

et al., 2009;Zhang et al., 2008b;Lim et al., 2011;Cheng et al., 2010;Shao et al., 2009a;Shao et al., 2009b;Xing et al., 2011). Recently, however, a modeling study by Li et al. (2013) in the Pearl River Delta region in China demonstrated the time dependence of ozone production regimes. Specifically, with high NOx emissions in the morning, the regional ozone production regime is categorized as VOC limited. In contrast, in the afternoon when the highest ozone concentrations are observed, a NOx limited regime is often found. The obvious issue to be addressed is that all of the above studies neglected how the uncertainty in hydroxyl radical chemistry would affect the ozone production regime evaluation. Moreover, HONO has been rarely constrained by observations in the previous modeling studies. Figure 5 shows the temporal variations of P_{H2O2}/P_{HNO3} from the all six different model scenarios. The VOC limited ozone formation regime was observed regardless of the HO_X simulation scenarios. Differences among different scenario are not noticeable in the morning when NO is high but noticeable differences can be noticed in the afternoon. In general, the model calculation results with faster HPALD formation rates indicate higher $P(H_2O_2)/P(HNO_3)$ in the afternoon. This analysis clearly shows that it is difficult to determine the appropriate policy implementation for NO_X or VOC controls to achieve ozone abatement in Asian megaticities without accurate understanding of radical isoprene interactions (e.g. Kim et al. (2013b)).

Another unresolved uncertainty in understanding tropospheric OH is its chemical loss rates. The limited observations of OH reactivity in BVOC dominant environments show consistent unaccounted OH chemical loss with observational datasets (Di Carlo et al., 2004;Edwards et al., 2013;Kim et al., 2011;Lou et al., 2010;Nolscher et al., 2012). Two different processes are speculated to cause unaccounted OH loss known as missing

OH reactivity: 1) primary emissions of unmeasured or unknown compounds and 2) oxidation products of well-known BVOCs especially isoprene. Most studies conducted in coniferous forests where monoterpenes are dominant primary BVOC emissions have concluded that unmeasured or unknown primary BVOC emissions caused missing OH reactivity (Sinha et al., 2010). On the other hand, studies conducted in isoprene dominant environments in mostly broadleaf or mixed forests concluded the main cause of missing OH reactivity as oxidation products of isoprene (Edwards et al., 2013;Kim et al., 2011). Edwards et al. (2013) presented a thorough analysis on potential impacts of isoprene oxidation products that are not routinely constrained by observations. The authors found significant contributions from secondary oxidation products such as multi-functional oxygenated compounds. Figure 6a shows the temporal variations of total OH reactivity calculated from five different model scenarios (I through V). The highest and the lowest OH reactivity levels were predicted from model calculations of Scenario V and Scenario II, respectively. This observation is directly correlated with calculated RO_2 levels as the lowest and highest RO_2 levels were calculated from Scenario II and Scenario V, respectively. Since VOC precursors and trace gases were all constrained by observations in the model calculations, the differences in model calculated OH reactivity should be mainly caused by the oxidation products of VOCs. This can be confirmed by the comparisons of model calculated formaldehyde concentrations from Scenario II and V as formaldehyde is a dominant oxidation product of isoprene (Figure 6b). The differences in formaldehyde levels suggest differences in OH reactivity levels from OVOCs in each model simulation. In summary, uncertainty in radical distributions especially RO_2 levels is directly propagated into uncertainty in OVOC formation.

These calculated results provide an upper limit of potential contributions from the oxidation products of the constrained VOC precursors considering that the box-model does not consider dry-deposition processes as Karl et al. (2010) and Edwards et al. (2013) suggested that there is significant uncertainty associated with the parameterizations of dry deposition especially OVOCs. Still, this analysis suggests that significant missing OH reactivity (~ up to factor of two to three) can be found without constraining OVOCs. OVOCs, especially multi-functional highly oxidized compounds are precursors for secondary organic aerosols (VOCs). Therefore, uncertainty surrounding missing OH reactivity significantly undermines our ability to constrain SOA formation and aerosol growth.

4. Summary and conclusion

We presented trace gas observation results from the TRF near the center of Seoul, South Korea. The dataset provides important constraints to evaluate the HO_X pool at the site where both anthropogenic and biogenic influences become important factors in determining oxidation capacity. Although the site is in the vicinity of a megacity with 25 million people, isoprene accounted for most of the OH loss from observed atmospheric hydrocarbon species during the 6-day focus period in early June 2012 during a regional pollution episode. In addition, observed NO_X levels were substantially lower than observed values in the center of the SMA. These observations indicate that impacts of aged pollution on BVOC photochemistry and aerosol formation can be observed at the TRF.

Six different model scenarios are employed to investigate the radical (OH, HO_2, and RO_2) distributions using the UWCM box-model. The observed trace gas data were constrained and the photochemical mechanisms (MCM 3.2) of seven VOC species with high levels at the TRF were integrated. The uncertainty in isoprene peroxy radical chemistry results in a wider range of OH, HO_2, and RO_2 distributions. Unconstrained HONO sources also cause a quite high level of underestimation in a radical pool ($OH+HO_2+RO_2$). OH simulation from the different model scenarios indicates much larger discrepancies (up to three times) than simulations for HO_2 and RO_2 (up to twice). OH is simulated in much higher levels with the consideration of an additional OH recycling channel from isoprene peroxy radical + HO_2 reactions and fast HPALD formation chemistry Peeters and Muller (2010). On the other hand, the RO_2 simulations indicate contrary results as HPALD formation depletes the RO_2 pool, which mostly composed by isoprene peroxy radicals. These results suggest that HO_2 and RO_2 observations can provide pivotal information about radical recycling and isoprene peroxy radical chemistry (Kim et al., 2013c;Wolfe et al., 2013). More studies on characterizing existing techniques to quantify HO_2 (Fuchs et al., 2011) and developing new techniques (Horstjann et al., 2013) are needed. In addition, the simulations with recently developed isoprene photo-oxidation chemistry show that radical termination processes (e.g. peroxide formation) get more efficient than radical recycling processes in the afternoon. This may come as a surprise as in general we expect the high NO_X conditions in the suburban regions of a megacity to have effective radical recycling. However, the critical factor determining competing reaction channels of recycling and peroxide formation is NO concentrations. Ratios of NO to NO_2 are not only correlated with NO_2 concentrations

and photolysis constants but also anti-correlated with RO_2, HO_2 and ozone concentrations and relevant kinetic constants as shown in (R6). Therefore, a semi-quantitative term such as the high 'NO_X' regime is not a proper term to define radical recycle regimes especially in high radical environments (e.g. HO_2 and RO_2) such as forest environments.

These uncertainties in estimating the radical pool size and distribution directly affect our ability for constraining photochemical ozone and OVOC production. The non-linear response of ozone production to NO_X and VOC abundances are determined by OH, HO_2, RO_2 and NO_2 concentrations. Regardless of which model calculation scenario we adapt, the TRF photochemical state appears to be a VOC limited ozone production regime. However, morning and afternoon show a very strong contrast with morning having a stronger degree of VOC limitation. In addition, a noticeable range of VOC sensitivity was calculated from the six different model scenarios especially in the afternoon. These analysis results, therefore, strongly indicate that uncertainty in radical photochemistry subsequently resulting in uncertainty in radical concentration estimations directly propagates in policy-making processes in effectiveness of NO_X or VOC controls in ozone reduction. In addition, OVOC production is predicted to significantly vary depending on the model simulation scenarios. As the fate of these OVOCs is uncertain and can include deposition, photolysis, or condensation, the implications of the uncertainty in OVOC production caused by the uncertainty in radical photochemistry should be addressed.

Acknowledgements

This research is financially supported by National Institute of Environmental Research of South Korea. The authors appreciate logistical supports from the research and supporting staff at Taehwa Research Forest operated by Seoul National University.

References

Apel, E. C., Riemer, D. D., Hills, A., Baugh, W., Orlando, J., Faloona, I., Tan, D., Brune, W., Lamb, B., Westberg, H., Carroll, M. A., Thornberry, T., and Geron, C. D.: Measurement and interpretation of isoprene fluxes and isoprene, methacrolein, and methyl vinyl ketone mixing ratios at the PROPHET site during the 1998 Intensive, J Geophys Res-Atmos, 107, Artn 4034 Doi 10.1029/2000jd000225, 2002.

Archibald, A. T., Jenkin, M. E., and Shallcross, D. E.: An isoprene mechanism intercomparison, Atmos Environ, 44, 5356-5364, Doi 10.1016/J.Atmosenv.2009.09.016, 2010.

Arneth, A., Schurgers, G., Lathiere, J., Duhl, T., Beerling, D. J., Hewitt, C. N., Martin, M., and Guenther, A.: Global terrestrial isoprene emission models: sensitivity to variability in climate and vegetation, Atmos Chem Phys, 11, 8037-8052, Doi 10.5194/Acp-11-8037-2011, 2011.

Bao, H., Shrestha, K. L., Kondo, A., Kaga, A., and Inoue, Y.: Modeling the influence of biogenic volatile organic compound emissions on ozone concentration during summer season in the Kinki region of Japan, Atmos Environ, 44, 421-431, Doi 10.1016/J.Atmosenv.2009.10.021, 2010.

Barket, D. J., Hurst, J. M., Couch, T. L., Colorado, A., Shepson, P. B., Riemer, D. D., Hills, A. J., Apel, E. C., Hafer, R., Lamb, B. K., Westberg, H. H., Farmer, C. T., Stabenau, E. R., and Zika, R. G.: Intercomparison of automated methodologies for determination of ambient isoprene during the PROPHET 1998 summer campaign, J Geophys Res-Atmos, 106, 24301-24313, Doi 10.1029/2000jd900562, 2001.

Blake, R. S., Monks, P. S., and Ellis, A. M.: Proton-Transfer Reaction Mass Spectrometry, Chem Rev, 109, 861-896, 2009.

Bryan, A. M., Bertman, S. B., Carroll, M. A., Dusanter, S., Edwards, G. D., Forkel, R., Griffith, S., Guenther, A. B., Hansen, R. F., Helmig, D., Jobson, B. T., Keutsch, F. N., Lefer, B. L., Pressley, S. N., Shepson, P. B., Stevens, P. S., and Steiner, A. L.: In-canopy gas-phase chemistry during CABINEX 2009: sensitivity of a 1-D canopy model to vertical mixing and isoprene chemistry, Atmos Chem Phys, 12, 8829-8849, Doi 10.5194/Acp-12-8829-2012, 2012.

Chameides, W. L., Lindsay, R. W., Richardson, J., and Kiang, C. S.: The Role of Biogenic Hydrocarbons in Urban Photochemical Smog - Atlanta as a Case-Study, Science, 241, 1473-1475, 1988.

Cheng, H. R., Guo, H., Saunders, S. M., Lam, S. H. M., Jiang, F., Wang, X. M., Simpson, I. J., Blake, D. R., Louie, P. K. K., and Wang, T. J.: Assessing photochemical ozone formation in the Pearl River Delta with a photochemical trajectory model, Atmos Environ, 44, 4199-4208, Doi 10.1016/J.Atmosenv.2010.07.019, 2010.

646 Crounse, J. D., Paulot, F., Kjaergaard, H. G., and Wennberg, P. O.: Peroxy radical
647 isomerization in the oxidation of isoprene, Phys Chem Chem Phys, 13, 13607-13613,
648 Doi 10.1039/C1cp21330j, 2011.
649 de Gouw, J., and Warneke, C.: Measurements of volatile organic compounds in the
650 earths atmosphere using proton-transfer-reaction mass spectrometry, Mass
651 Spectrom Rev, 26, 223-257, 2007.
652 Di Carlo, P., Brune, W. H., Martinez, M., Harder, H., Lesher, R., Ren, X. R., Thornberry,
653 T., Carroll, M. A., Young, V., Shepson, P. B., Riemer, D., Apel, E., and Campbell, C.:
654 Missing OH reactivity in a forest: Evidence for unknown reactive biogenic VOCs,
655 Science, 304, 722-725, Doi 10.1126/Science.1094392, 2004.
656 Edwards, P. M., Evans, M. J., Furneaux, K. L., Hopkins, J., Ingham, T., Jones, C., Lee, J.
657 D., Lewis, A. C., Moller, S. J., Stone, D., Whalley, L. K., and Heard, D. E.: OH reactivity in
658 a South East Asian tropical rainforest during the Oxidant and Particle Photochemical
659 Processes (OP3) project, Atmos Chem Phys, 13, 9497-9514, Doi 10.5194/Acp-13-
660 9497-2013, 2013.
661 Fuchs, H., Bohn, B., Hofzumahaus, A., Holland, F., Lu, K. D., Nehr, S., Rohrer, F., and
662 Wahner, A.: Detection of HO2 by laser-induced fluorescence: calibration and
663 interferences from RO2 radicals, Atmos Meas Tech, 4, 1209-1225, Doi 10.5194/Amt-
664 4-1209-2011, 2011.
665 Guenther, A.: Biological and chemical diversity of biogenic volatile organic emissions
666 into the atmosphere, Atmospheric Sciences, 2013, ArticleID 786290, 2013.
667 Hao, N., Zhou, B., Chen, D., and Chen, L. M.: Observations of nitrous acid and its
668 relative humidity dependence in Shanghai, J Environ Sci-China, 18, 910-915, Doi
669 10.1016/S1001-0742(06)60013-2, 2006.
670 Hofzumahaus, A., Rohrer, F., Lu, K. D., Bohn, B., Brauers, T., Chang, C. C., Fuchs, H.,
671 Holland, F., Kita, K., Kondo, Y., Li, X., Lou, S. R., Shao, M., Zeng, L. M., Wahner, A., and
672 Zhang, Y. H.: Amplified Trace Gas Removal in the Troposphere, Science, 324, 1702-
673 1704, 10.1126/science.1164566, 2009.
674 Horstjann, M., Andres Hernandez, M. D., Nenakhov, V., Chrobry, A., and Burrows, J.
675 P.: Peroxy radical detection for airborne atmospheric measurements using cavity
676 ehnaced absorption spectroscopy of NO2, Atmospheric Measurement Techniques
677 Discussion, 6, 9655-9688, 2013.
678 Huang, M., Bowman, K. W., Carmichael, G. R., Pierce, R. B., Worden, H. M., Luo, M.,
679 Cooper, O. R., Pollack, I. B., Ryerson, T. B., and Brown, S. S.: Impact of Southern
680 California anthropogenic emissions on ozone pollution in the mountain states:
681 Model analysis and observational evidence from space, J Geophys Res-Atmos, 118,
682 12784-12803, Doi 10.1002/2013jd020205, 2013.
683 Karl, T., Harley, P., Emmons, L., Thornton, B., Guenther, A., Basu, C., Turnipseed, A.,
684 and Jardine, K.: Efficient Atmospheric Cleansing of Oxidized Organic Trace Gases by
685 Vegetation, Science, 330, 816-819, Doi 10.1126/Science.1192534, 2010.
686 Kim, K. H., Ho, D. X., Park, C. G., Ma, C. J., Pandey, S. K., Lee, S. C., Jeong, H. J., and Lee, S.
687 H.: Volatile Organic Compounds in Ambient Air at Four Residential Locations in
688 Seoul, Korea, Environ Eng Sci, 29, 875-889, Doi 10.1089/Ees.2011.0280, 2012.
689 Kim, S., Karl, T., Guenther, A., Tyndall, G., Orlando, J., Harley, P., Rasmussen, R., and
690 Apel, E.: Emissions and ambient distributions of Biogenic Volatile Organic

691 Compounds (BVOC) in a ponderosa pine ecosystem: interpretation of PTR-MS mass
692 spectra, Atmos Chem Phys, 10, 1759-1771, 2010.
693 Kim, S., Guenther, A., Karl, T., and Greenberg, J.: Contributions of primary and
694 secondary biogenic VOC tototal OH reactivity during the CABINEX (Community
695 Atmosphere-Biosphere INteractions Experiments)-09 field campaign, Atmos Chem
696 Phys, 11, 8613-8623, 2011.
697 Kim, S., Guenther, A., and Apel, E.: Quantitative and qualitative sensing techniques
698 for biogenic volatile organic compounds and their oxidation products, Environ Sci-
699 Proc Imp, 15, 1301-1314, Doi 10.1039/C3em00040k, 2013a.
700 Kim, S., Lee, M., Kim, S., Choi, S., Seok, S., and Kim, S.: Photochemical characteristics
701 of high and low ozone episodes observed in the Taehwa Forest observatory (TFO) in
702 June 2011 near Seoul South Korea, Asia-Pacific Journal of Atmospheric Sciences, 49,
703 325-331, Doi 10.1007/S13143-013-0031-0, 2013b.
704 Kim, S., Wolfe, G. M., Mauldin, L., Cantrell, C., Guenther, A., Karl, T., Turnipseed, A.,
705 Greenberg, J., Hall, S. R., Ullmann, K., Apel, E., Hornbrook, R., Kajii, Y., Nakashima, Y.,
706 Keutsch, F. N., DiGangi, J. P., Henry, S. B., Kaser, L., Schnitzhofer, R., Graus, M., Hansel,
707 A., Zheng, W., and Flocke, F. F.: Evaluation of HOx sources and cycling using
708 measurement-constrained model calculations in a 2-methyl-3-butene-2-ol (MBO)
709 and monoterpene (MT) dominated ecosystem, Atmos Chem Phys, 13, 2031-2044,
710 Doi 10.5194/Acp-13-2031-2013, 2013c.
711 Kim, S., VandenBoer, T. C., Young, C. J., Riedel, T. P., Thornton, J. A., Swarthout, B.,
712 Sive, B., Lerner, B., Gilman, J. B., Warneke, C., Roberts, J. M., Guenther, A., Wagner, N.
713 L., Dube, W. P., Williams, E., and Brown, S. S.: The primary and recycling sources of
714 OH during the NACHTT-2011 campaign: HONO as an important OH primary source
715 in the wintertime, J Geophys Res-Atmos, 119, 6886-6896, Doi
716 10.1002/2013jd019784, 2014.
717 Kim, S. Y., Jiang, X. Y., Lee, M., Turnipseed, A., Guenther, A., Kim, J. C., Lee, S. J., and
718 Kim, S.: Impact of biogenic volatile organic compounds on ozone production at the
719 Taehwa Research Forest near Seoul, South Korea, Atmos Environ, 70, 447-453, Doi
720 10.1016/J.Atmosenv.2012.11.005, 2013d.
721 Lelieveld, J., Butler, T. M., Crowley, J. N., Dillon, T. J., Fischer, H., Ganzeveld, L., Harder,
722 H., Lawrence, M. G., Martinez, M., Taraborrelli, D., and Williams, J.: Atmospheric
723 oxidation capacity sustained by a tropical forest, Nature, 452, 737-740, 2008.
724 Levy, H.: Normal Atmosphere - Large Radical and Formaldehyde Concentrations
725 Predicted, Science, 173, 141-143, 1971.
726 Li, X., Brauers, T., Haseler, R., Bohn, B., Fuchs, H., Hofzumahaus, A., Holland, F., Lou,
727 S., Lu, K. D., Rohrer, F., Hu, M., Zeng, L. M., Zhang, Y. H., Garland, R. M., Su, H., Nowak,
728 A., Wiedensohler, A., Takegawa, N., Shao, M., and Wahner, A.: Exploring the
729 atmospheric chemistry of nitrous acid (HONO) at a rural site in Southern China,
730 Atmos Chem Phys, 12, 1497-1513, Doi 10.5194/Acp-12-1497-2012, 2012.
731 Li, Y., Lau, A. K. H., Fung, J. C. H., Zheng, J. Y., and Liu, S. C.: Importance of NOx control
732 for peak ozone reduction in the Pearl River Delta region, J Geophys Res-Atmos, 118,
733 9428-9443, Doi 10.1002/Jgrd.50659, 2013.
734 Lim, Y. J., Armendariz, A., Son, Y. S., and Kim, J. C.: Seasonal variations of isoprene
735 emissions from five oak tree species in East Asia, Atmos Environ, 45, 2202-2210, Doi
736 10.1016/J.Atmosenv.2011.01.066, 2011.

737 Liu, Y. J., Herdlinger-Blatt, I., McKinney, K. A., and Martin, S. T.: Production of methyl
738 vinyl ketone and methacrolein via the hydroperoxyl pathway of isoprene oxidation,
739 Atmos Chem Phys, 13, 5715-5730, Doi 10.5194/Acp-13-5715-2013, 2013.
740 Lou, S., Holland, F., Rohrer, F., Lu, K., Bohn, B., Brauers, T., Chang, C. C., Fuchs, H.,
741 Haseler, R., Kita, K., Kondo, Y., Li, X., Shao, M., Zeng, L., Wahner, A., Zhang, Y., Wang,
742 W., and Hofzumahaus, A.: Atmospheric OH reactivities in the Pearl River Delta -
743 China in summer 2006: measurement and model results, Atmos Chem Phys, 10,
744 11243-11260, 2010.
745 Lu, K. D., Rohrer, F., Holland, F., Fuchs, H., Bohn, B., Brauers, T., Chang, C. C., Haseler,
746 R., Hu, M., Kita, K., Kondo, Y., Li, X., Lou, S. R., Nehr, S., Shao, M., Zeng, L. M., Wahner,
747 A., Zhang, Y. H., and Hofzumahaus, A.: Observation and modelling of OH and HO2
748 concentrations in the Pearl River Delta 2006: a missing OH source in a VOC rich
749 atmosphere, Atmos Chem Phys, 12, 1541-1569, Doi 10.5194/Acp-12-1541-2012,
750 2012.
751 Ma, J. Z., Wang, W., Chen, Y., Liu, H. J., Yan, P., Ding, G. A., Wang, M. L., Sun, J., and
752 Lelieveld, J.: The IPAC-NC field campaign: a pollution and oxidization pool in the
753 lower atmosphere over Huabei, China, Atmos Chem Phys, 12, 3883-3908, Doi
754 10.5194/Acp-12-3883-2012, 2012.
755 Mao, J., Ren, X., Zhang, L., Van Duin, D. M., Cohen, R. C., Park, J. H., Goldstein, A. H.,
756 Paulot, F., Beaver, M. R., Crounse, J. D., Wennberg, P. O., DiGangi, J. P., Henry, S. B.,
757 Keutsch, F. N., Park, C., Schade, G. W., Wolfe, G. M., Thornton, J. A., and Brune, W. H.:
758 Insights into hydroxyl measurements and atmospheric oxidation in a California
759 forest, Atmos Chem Phys, 12, 8009-8020, Doi 10.5194/Acp-12-8009-2012, 2012.
760 Mao, J. Q., Ren, X. R., Chen, S. A., Brune, W. H., Chen, Z., Martinez, M., Harder, H., Lefer,
761 B., Rappengluck, B., Flynn, J., and Leuchner, M.: Atmospheric oxidation capacity in
762 the summer of Houston 2006: Comparison with summer measurements in other
763 metropolitan studies, Atmos Environ, 44, 4107-4115, Doi
764 10.1016/J.Atmosenv.2009.01.013, 2010.
765 Na, K., and Kim, Y. P.: Seasonal characteristics of ambient volatile organic
766 compounds in Seoul, Korea, Atmos Environ, 35, 2603-2614, Doi 10.1016/S1352-
767 2310(00)00464-7, 2001.
768 NIER: Annual Report for Atmospheric Environment, National Insititute of
769 Environmetal Rsearch, 2010.
770 Nolscher, A. C., Williams, J., Sinha, V., Custer, T., Song, W., Johnson, A. M., Axinte, R.,
771 Bozem, H., Fischer, H., Pouvesle, N., Phillips, G., Crowley, J. N., Rantala, P., Rinne, J.,
772 Kulmala, M., Gonzales, D., Valverde-Canossa, J., Vogel, A., Hoffmann, T., Ouwersloot,
773 H. G., de Arellano, J. V. G., and Lelieveld, J.: Summertime total OH reactivity
774 measurements from boreal forest during HUMPPA-COPEC 2010, Atmos Chem Phys,
775 12, 8257-8270, Doi 10.5194/Acp-12-8257-2012, 2012.
776 Oswald, R., Behrendt, T., Ermel, M., Wu, D., Su, H., Cheng, Y., Breuninger, C., Moravek,
777 A., Mougin, E., Delon, C., Loubet, B., Pommerening-Roser, A., Sorgel, M., Poschl, U.,
778 Hoffmann, T., Andreae, M. O., Meixner, F. X., and Trebs, I.: HONO Emissions from Soil
779 Bacteria as a Major Source of Atmospheric Reactive Nitrogen, Science, 341, 1233-
780 1235, Doi 10.1126/Science.1242266, 2013.

781 Paulot, F., Crounse, J. D., Kjaergaard, H. G., Kroll, J. H., Seinfeld, J. H., and Wennberg, P.
782 O.: Isoprene photooxidation: new insights into the production of acids and organic
783 nitrates, Atmos Chem Phys, 9, 1479-1501, 2009.
784 Paulson, S. E., and Seinfeld, J. H.: Development and evaluation of a photooxidation
785 mechanism for isoprene, Journal of Geophysical Research, 97, 20703-20715, 1992.
786 Peeters, J., and Muller, J. F.: HOx radical regeneration in isoprene oxidation via
787 peroxy radical isomerisations. II: experimental evidence and global impact, Phys
788 Chem Chem Phys, 12, 14227-14235, Doi 10.1039/C0cp00811g, 2010.
789 Pollack, I. B., Ryerson, T. B., Trainer, M., Neuman, J. A., Roberts, J. M., and Parrish, D.
790 D.: Trends in ozone, its precursors, and related secondary oxidation products in Los
791 Angeles, California: A synthesis of measurements from 1960 to 2010, J Geophys Res-
792 Atmos, 118, 5893-5911, Doi 10.1002/Jgrd.50472, 2013.
793 Ran, L., Zhao, C. S., Xu, W. Y., Lu, X. Q., Han, M., Lin, W. L., Yan, P., Xu, X. B., Deng, Z. Z.,
794 Ma, N., Liu, P. F., Yu, J., Liang, W. D., and Chen, L. L.: VOC reactivity and its effect on
795 ozone production during the HaChi summer campaign, Atmos Chem Phys, 11, 4657-
796 4667, Doi 10.5194/Acp-11-4657-2011, 2011.
797 Ren, X., Sanders, J. E., Rajendran, A., Weber, R. J., Goldstein, A. H., Pusede, S. E.,
798 Browne, E. C., Min, K. E., and Cohen, R. C.: A relaxed eddy accumulation system for
799 measuring vertical fluxes of nitrous acid, Atmos Meas Tech, 4, 2093-2103, Doi
800 10.5194/Amt-4-2093-2011, 2011.
801 Ryerson, T. B., Andrews, A. E., Angevine, W. M., Bates, T. S., Brock, C. A., Cairns, B.,
802 Cohen, R. C., Cooper, O. R., de Gouw, J. A., Fehsenfeld, F. C., Ferrare, R. A., Fischer, M.
803 L., Flagan, R. C., Goldstein, A. H., Hair, J. W., Hardesty, R. M., Hostetler, C. A., Jimenez, J.
804 L., Langford, A. O., McCauley, E., McKeen, S. A., Molina, L. T., Nenes, A., Oltmans, S. J.,
805 Parrish, D. D., Pederson, J. R., Pierce, R. B., Prather, K., Quinn, P. K., Seinfeld, J. H.,
806 Senff, C. J., Sorooshian, A., Stutz, J., Surratt, J. D., Trainer, M., Volkamer, R., Williams, E.
807 J., and Wofsy, S. C.: The 2010 California Research at the Nexus of Air Quality and
808 Climate Change (CalNex) field study, J Geophys Res-Atmos, 118, 5830-5866, Doi
809 10.1002/Jgrd.50331, 2013.
810 Ryu, Y. H., Baik, J. J., Kwak, K. H., Kim, S., and Moon, N.: Impacts of urban land-surface
811 forcing on ozone air quality in the Seoul metropolitan area, Atmos Chem Phys, 13,
812 2177-2194, Doi 10.5194/Acp-13-2177-2013, 2013.
813 Sartelet, K. N., Couvidat, F., Seigneur, C., and Roustan, Y.: Impact of biogenic
814 emissions on air quality over Europe and North America, Atmos Environ, 53, 131-
815 141, Doi 10.1016/J.Atmosenv.2011.10.046, 2012.
816 Seinfeld, J. H.: Urban Air-Pollution - State of the Science, Science, 243, 745-752, Doi
817 10.1126/Science.243.4892.745, 1989.
818 Shao, M., Lu, S. H., Liu, Y., Xie, X., Chang, C. C., Huang, S., and Chen, Z. M.: Volatile
819 organic compounds measured in summer in Beijing and their role in ground-level
820 ozone formation, J Geophys Res-Atmos, 114, Artn D00g06
821 Doi 10.1029/2008jd010863, 2009a.
822 Shao, M., Zhang, Y. H., Zeng, L. M., Tang, X. Y., Zhang, J., Zhong, L. J., and Wang, B. G.:
823 Ground-level ozone in the Pearl River Delta and the roles of VOC and NO(x) in its
824 production, J Environ Manage, 90, 512-518, Doi 10.1016/J.Jenvman.2007.12.008,
825 2009b.

826 Sillman, S., and He, D.: Some theoretical results concerning O3-NOx-VOC chemistry
827 and NOx-VOC indicators, Journal of Geophysical Research, 107,
828 4659,doi:4610.1029:2001JD001123, 2002.
829 Sinha, V., Williams, J., Lelieveld, J., Ruuskanen, T. M., Kajos, M. K., Patokoski, J., Hellen,
830 H., Hakola, H., Mogensen, D., Boy, M., Rinne, J., and Kulmala, M.: OH Reactivity
831 Measurements within a Boreal Forest: Evidence for Unknown Reactive Emissions,
832 Environ Sci Technol, 44, 6614-6620, Doi 10.1021/Es101780b, 2010.
833 Song, C. H., Park, M. E., Lee, E. J., Lee, J. H., Lee, B. K., Lee, D. S., Kim, J., Han, J. S., Moon,
834 K. J., and Kondo, Y.: Possible particulate nitrite formation and its atmospheric
835 implications inferred from the observations in Seoul, Korea, Atmos Environ, 43,
836 2168-2173, Doi 10.1016/J.Atmosenv.2009.01.018, 2009.
837 Tie, X., Geng, F., Guenther, A., Cao, J., Greenberg, J., Zhang, R., Apel, E., Li, G.,
838 Weinheimer, A., Chen, J., and Cai, C.: Megacity impacts on regional ozone formation:
839 observations and WRF-Chem modeling for the MIRAGE-Shanghai field campaign,
840 Atmos Chem Phys, 13, 5655-5669, Doi 10.5194/Acp-13-5655-2013, 2013.
841 Tonnesen, G. S., and Dennis, R. L.: Analysis of radical propagation efficiency to assess
842 ozone sensitivity to hydrocarbons and NOx 2. Long-lived species as indicators of
843 ozone concentration sensitivity, J Geophys Res-Atmos, 105, 9227-9241, Doi
844 10.1029/1999jd900372, 2000a.
845 Tonnesen, G. S., and Dennis, R. L.: Analysis of radical propagation efficiency to assess
846 ozone sensitivity to hydrocarbons and NOx 1. Local indicators of instantaneous odd
847 oxygen production sensitivity, J Geophys Res-Atmos, 105, 9213-9225, Doi
848 10.1029/1999jd900371, 2000b.
849 Trainer, M., Williams, E., Parrish, D. D., Buhr, M. P., Allwine, E. J., Westberg, H.,
850 Fehsenfeld, F. C., and Liu, S. C.: Models and observations of the impact of natural
851 hydrocarbons on rural ozone, Nature, 329, 705 - 707, 1987.
852 Tseng, K. H., Wang, J. L., Cheng, M. T., and Tsuang, B. J.: Assessing the Relationship
853 between Air Mass Age and Summer Ozone Episodes Based on Photochemical
854 Indices, Aerosol Air Qual Res, 9, 149-171, 2009.
855 VandenBoer, T., Murphy, J. G., Roberts, J. M., Middlebrook, A. M., Brock, C., Lerner, B.
856 M., Wolfe, D. E., Williams, E., Brown, S. S., Warneke, C., De Gouw, J., Wagner, N. L.,
857 Young, C. C., Dube, W. P., Bahreini, R., Riedel, T., Thornton, J. A., Ozturk, F., Keene, W.,
858 Maben, J. R., Pszenny, A., Kim, S., Grossberg, N., and Lefer, B.: Understanding the role
859 of the ground surface in HONO vertical structure: High resolution vertical profiles
860 during NACHTT-11, submitted, 2013.
861 Wolfe, G. M., and Thornton, J. A.: The chemistry of atmosphere-forest exchange
862 (CAFE) model - PART1: Model description and characterization, Atmos Chem Phys,
863 11, 77-101, 2011.
864 Wolfe, G. M., Crounse, J. D., Parrish, J. D., St Clair, J. M., Beaver, M. R., Paulot, F., Yoon,
865 T. P., Wennberg, P. O., and Keutsch, F. N.: Photolysis, OH reactivity and ozone
866 reactivity of a proxy for isoprene-derived hydroperoxyenals (HPALDs), Phys Chem
867 Chem Phys, 14, 7276-7286, 2012.
868 Wolfe, G. M., Cantrell, C., Kim, S., Mauldin, R., Karl, T., Harley, P., Turnipseed, A.,
869 Zheng, W., Flocke, F., Apel, E., Hornbrook, R. S., Hall, S., Ullmann, K., Henry, S. B.,
870 Digangi, J., Boyle, E. S., Kaser, L., Schnitzhofer, R., Hansel, A., Graus, M., Nakashima, Y.,
871 Kajii, Y., Guenther, A., and Keutsch, F.: Missing peroxy radical sources within a rural

forest canopy, Atmospheric Chemistry and Physics Discussion, 13, 31713-31759, 2013.
Wong, K. W., Tsai, C., Lefer, B., Haman, C., Grossberg, N., Brune, W. H., Ren, X., Luke, W., and Stutz, J.: Daytime HONO vertical gradients during SHARP 2009 in Houston, TX, Atmos Chem Phys, 12, 635-652, Doi 10.5194/Acp-12-635-2012, 2012.
Xing, J., Wang, S. X., Jang, C., Zhu, Y., and Hao, J. M.: Nonlinear response of ozone to precursor emission changes in China: a modeling study using response surface methodology, Atmos Chem Phys, 11, 5027-5044, Doi 10.5194/Acp-11-5027-2011, 2011.
Yoshino, A., Nakashima, Y., Miyazaki, K., Kato, S., Suthawaree, J., Shimo, N., Matsunaga, S., Chatani, S., Apel, E., Greenberg, J., Guenther, A., Ueno, H., Sasaki, H., Hoshi, J., Yokota, H., Ishii, K., and Kajii, Y.: Air quality diagnosis from comprehensive observations of total OH reactivity and reactive trace species in urban central Tokyo, Atmos Environ, 49, 51-59, Doi 10.1016/J.Atmosenv.2011.12.029, 2012.
Zhang, Y., Hu, X. M., Leung, L. R., and Gustafson, W. I.: Impacts of regional climate change on biogenic emissions and air quality, J Geophys Res-Atmos, 113, Artn D18310
Doi 10.1029/2008jd009965, 2008a.
Zhang, Y. H., Su, H., Zhong, L. J., Cheng, Y. F., Zeng, L. M., Wang, X. S., Xiang, Y. R., Wang, J. L., Gao, D. F., Shao, M., Fan, S. J., and Liu, S. C.: Regional ozone pollution and observation-based approach for analyzing ozone-precursor relationship during the PRIDE-PRD2004 campaign, Atmos Environ, 42, 6203-6218, Doi 10.1016/J.Atmosenv.2008.05.002, 2008b.
Zhao, J., and Zhang, R. Y.: Proton transfer reaction rate constants between hydronium ion (H3O(+)) and volatile organic compounds, Atmos Environ, 38, 2177-2185, 2004.
Zhou, X. L., Zhang, N., TerAvest, M., Tang, D., Hou, J., Bertman, S., Alaghmand, M., Shepson, P. B., Carroll, M. A., Griffith, S., Dusanter, S., and Stevens, P. S.: Nitric acid photolysis on forest canopy surface as a source for tropospheric nitrous acid, Nat Geosci, 4, 440-443, Doi 10.1038/Ngeo1164, 2011.

904 Table 1. Analytical characteristics of trace gas analyzers at TRF

905

Chemical Species	Manufacturer and Model Number	Uncertainty	Lower Limit of Detection
CO	Thermo Scientific 48i TLE	10%	40 ppb
NO_X	Thermo Scientific 42i-TL	15%	50 ppt
SO_2	Thermo Scientific 43i-TLE	10%	50 ppt
ozone	Thermo Scientific 49i	5%	< 1 ppb

906
907

Table 2. Terpenoid speciation analysis results from GC-MS a) branch enclosure and b) ambient air samples.

a)

Terpenoids	*Composition(%)	Speciation	*Composition(%)
Isoprene	0.5		
Monoterpenes	92.9	α-pinene	36.7
		camphene	13.1
		β-pinene	12.0
		β-myrcene	27.7
		α-terpinolene	1.9
		d-limonene	8.6
Sesquiterpenes	6.6	β-caryophyllene	53.2
		α-caryophyllene	46.8

b)

Terpeniods	*Composition(%)	Speciation	*Composition(%)
Monoterpenes	98.6	α-pinene	38.8
		β-piene	36.5
		camphene	13.5
		d-limonene	11
Sesquiterpenes	1.4	longifolene	100

*Composition is calculated based on the mixing ratio scale

Table 3. A summary of critical differences in input parameters for four different model simulation scenarios presented in this study

	HPALD chemistry	*α	Observational Constraints
Scenario I	No	0	-All
Scenario II	#Peeters and Muller (2010)	0	-All
Scenario III	+Crounse et al. (2011)	0	-All
Scenario IV	#Peeters and Muller (2010)	2.6	-All
Scenario V	+Crounse et al. (2011)	2.6	-All
Scenario VI	#Peeters and Muller (2010)	2.6	-All but HONO

*α is an OH yield from reactions between an isoprene peroxy radical and HO_2, #k298 = ~ 0.08 for isoprene peroxy radical isomerization rate leading to produce HPALD, +k298 = 0.002 for isoprene peroxy radical isomerization rate, -All the observed diurnal variations, appeared in Figure 1 are constrained in the model along with ambient pressure and humidity.

Table 4 A summary for radical distributions from the observationally constrained box-model simulation results

	OH		HO_2		RO_2		Constraints
Local Time	8:00-12:00	13:00-16:00	8:00-12:00	13:00-16:00	8:00-12:00	13:00-16:00	
Scenario I	3.85×10^6	3.08×10^6	4.10×10^8	7.02×10^8	3.65×10^8	1.14×10^9	All
Scenario II	3.99×10^6	3.69×10^6	3.99×10^8	7.86×10^8	3.51×10^8	9.62×10^8	All
Scenario III	3.86×10^6	3.13×10^6	4.09×10^8	7.09×10^8	3.64×10^8	1.12×10^9	All
Scenario IV	4.27×10^6	4.49×10^6	4.29×10^8	8.70×10^8	3.66×10^8	1.06×10^9	All
Scenario V	4.21×10^6	4.52×10^6	4.55×10^8	8.55×10^8	3.86×10^8	1.28×10^9	All
Scenario VI	1.61×10^6	1.61×10^6	1.95×10^8	4.82×10^8	1.75×10^8	7.25×10^8	All but HONO
Scenario VII	1.82×10^6	2.55×10^6	2.09×10^8	6.07×10^8	1.80×10^8	7.00×10^8	All but HONO

unit: molecules cm^{-3}

Figure 1. Averaged temporal variations observed trace gases at TRF (June 1st to June 6th, 2012).

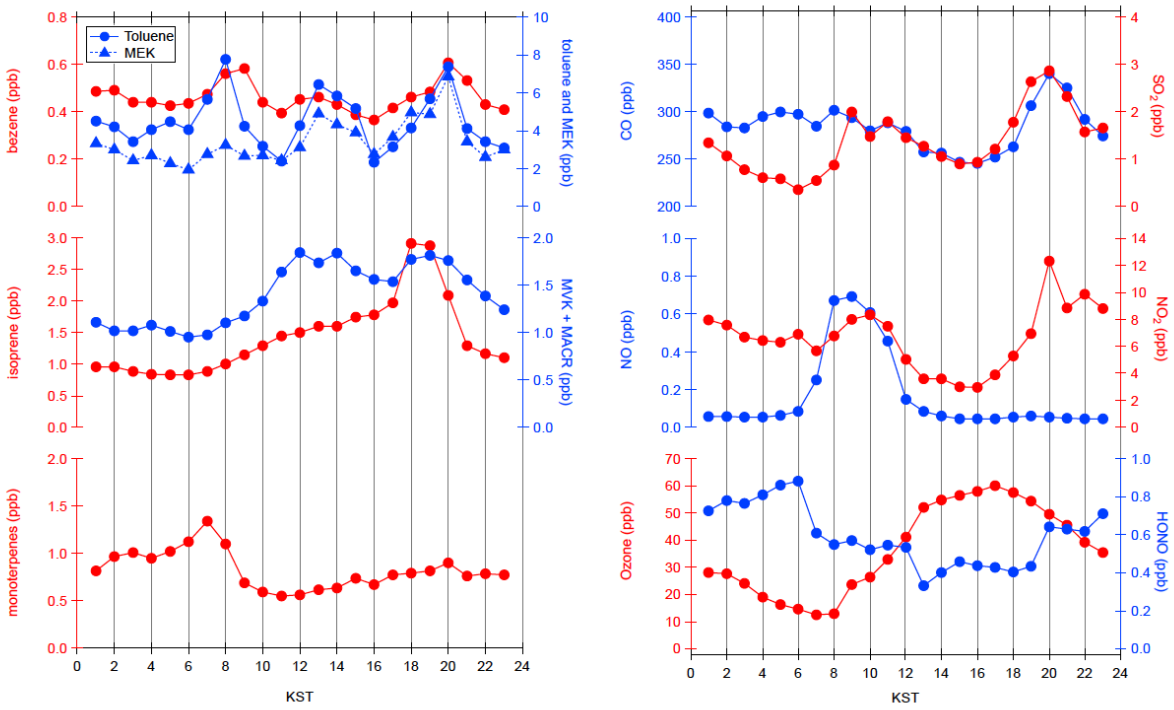

Figure 2. The temporal variations of OH reactivity calculated from the observed dataset at TRF (Figure 1). KST means Korean Standard Time (GMT+9).

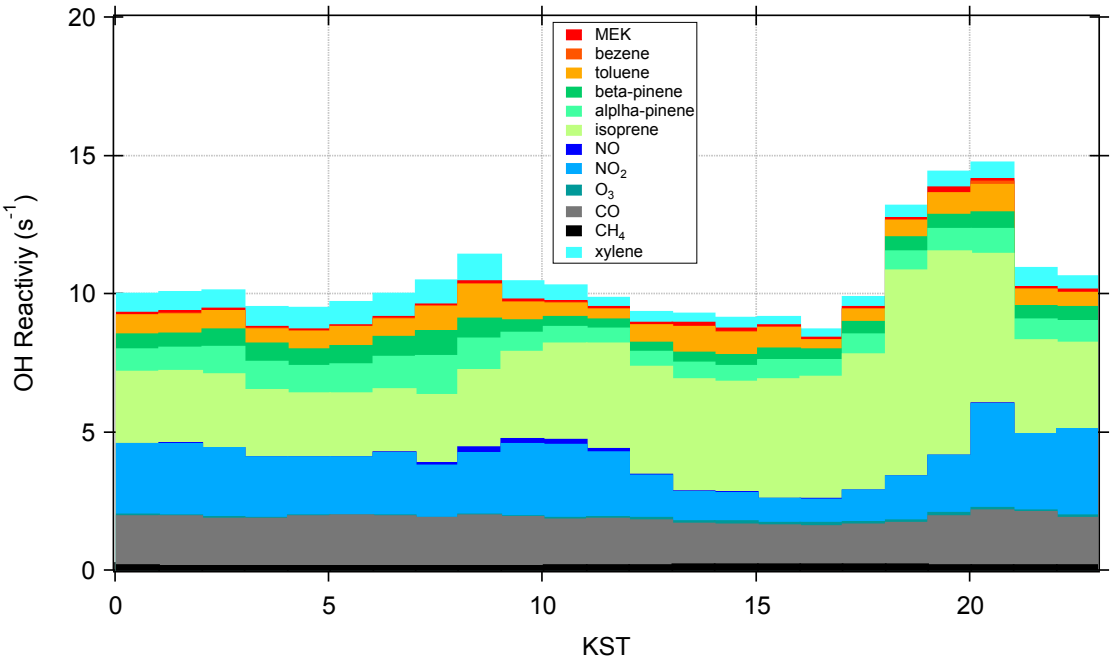

Figure 3. The temporal variations of OH, HO_2, and RO_2 calculated by six different observationally constrained UWCM box model scenarios.

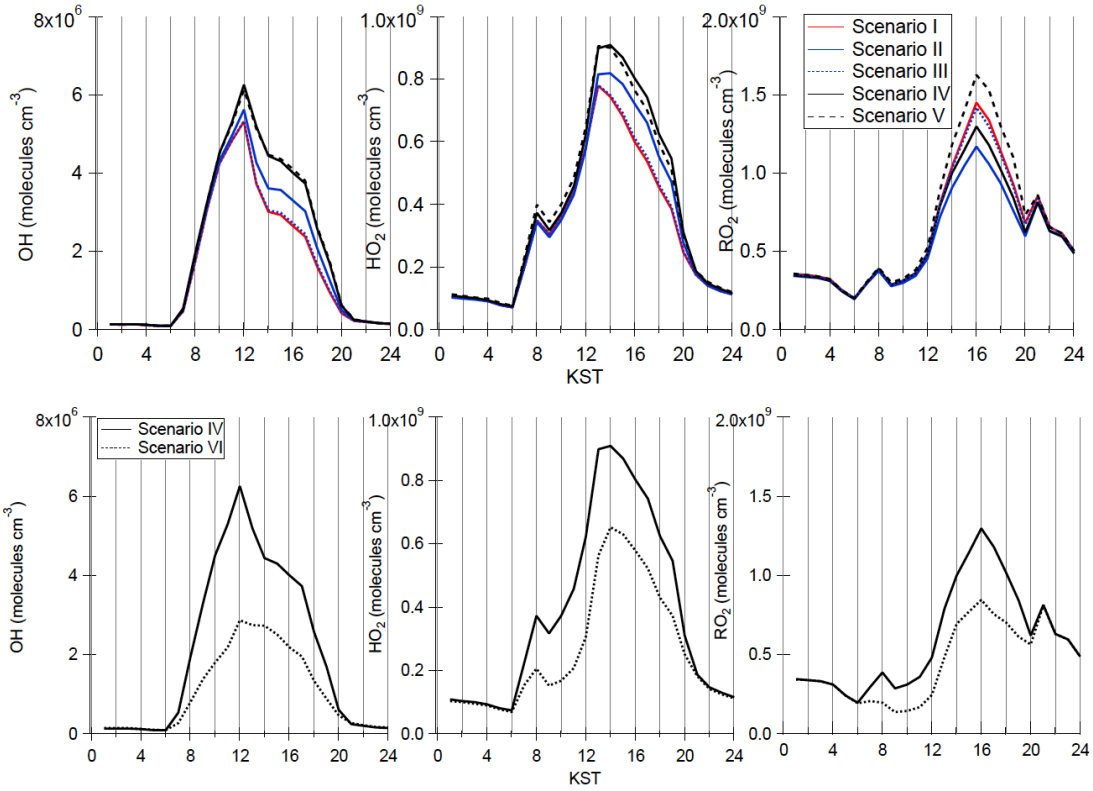

Figure 4 The temporal variations of radical recycling (red) and destruction (blue, black and green) rates calculated using the UWCM box model for different model scenarios

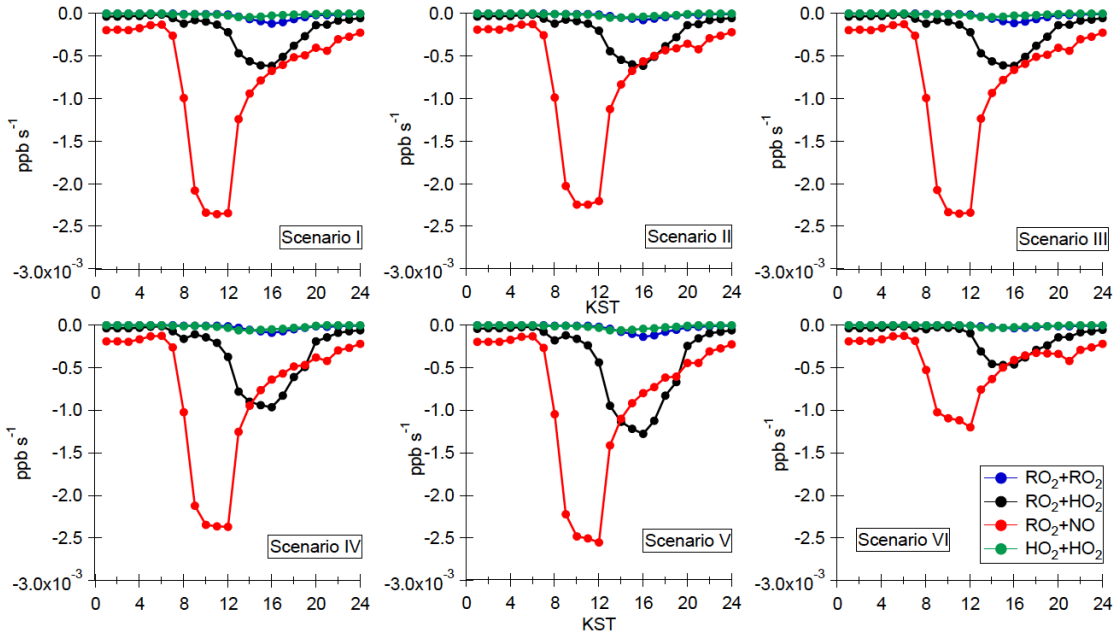

Figure 5. The temporal variations of P_{H2O2}/P_{HNO3} calculated from the UWCM box model from six different model scenarios

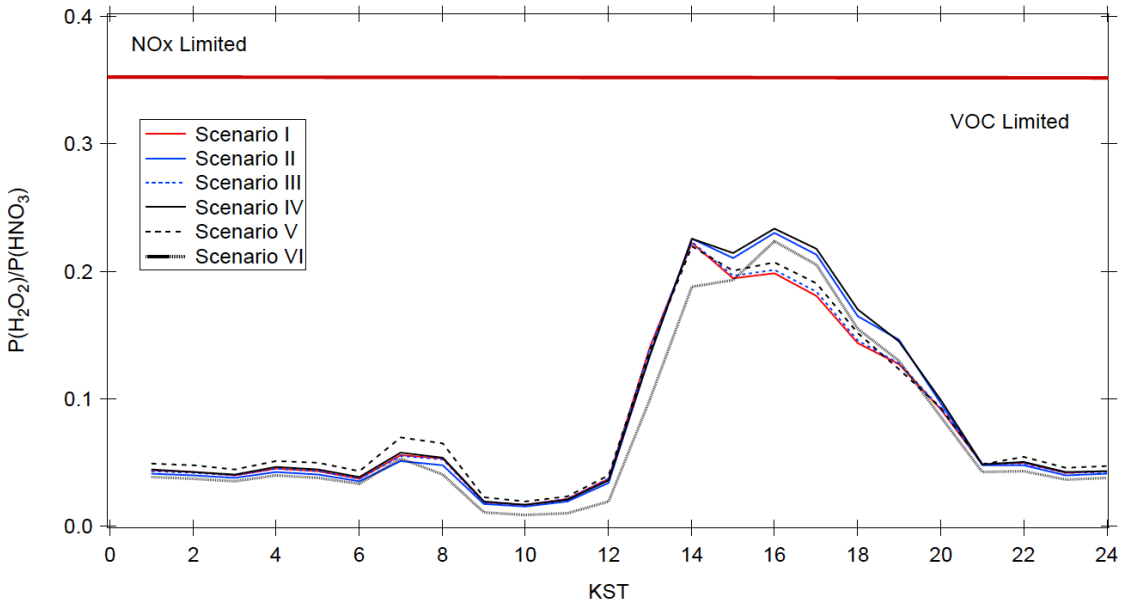

989 Figure 6. The temporal distributions of UWCM calculated OH reactivity (top panel) and
990 formaldehyde (bottom panel)
991
992
993
994

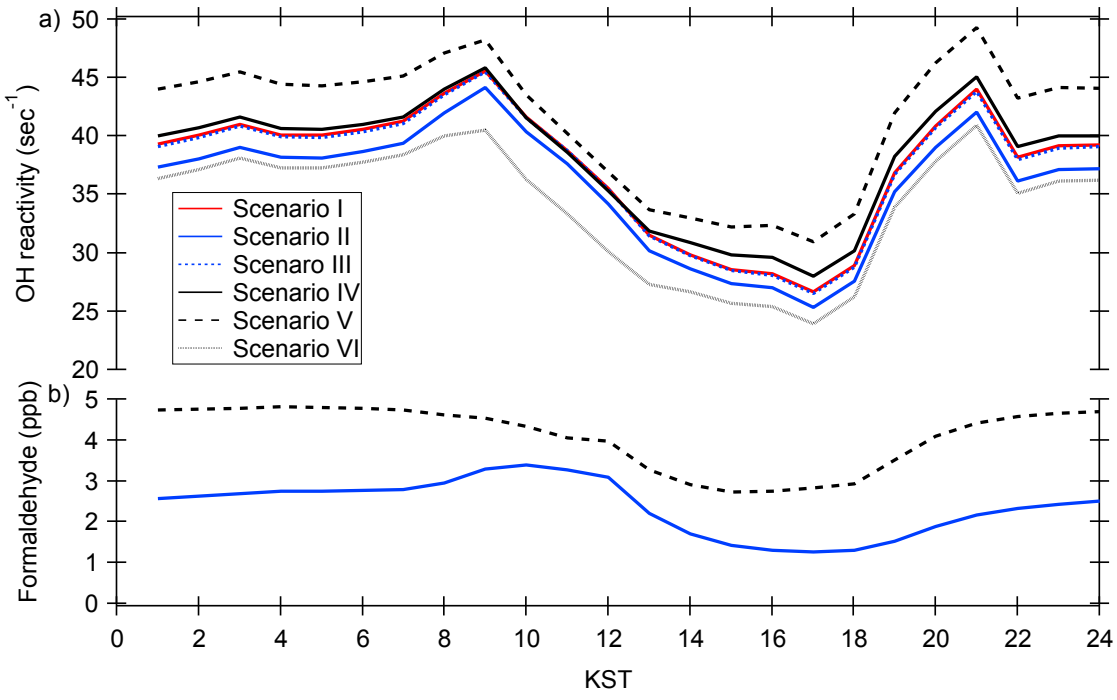

995